Stansfield E, Kumar K, Mitteroecker P, Grunstra NDS (2021). Biomechanical trade-offs in the pelvic floor constrain the evolution of the human birth canal. *PNAS*, 118(16), e2022159118.

SI Appendix

Analytical solution for large deflection of the pelvic floor

This section provides an analytical solution for an idealized circular pelvic floor membrane with a uniform thickness subjected to a normal pressure undergoing large deflections. For small deflection, the resistance to bending dominates deflection behavior [1]. The deflection δof a circular pelvic floor fixed all around under a uniform pressure *P* is written as:

$$\delta(r) = \frac{Pa^4}{64\,\alpha}\left[1 - \left(\frac{r}{a}\right)^2\right]^2 \quad (1)$$

where *r* and *a* are the radial distance and the radius of the pelvic floor. αis the flexural rigidity and is defined as

$\alpha = \frac{E\,t^3}{12\,(1-\nu^2)}$, where *E* is Young's modulus, *t* is the thickness of the pelvic floor and νis the Poisson's ratio.

In contrast to small deflection theory, deflections in the pelvic floor are analogous to membrane theory dominated by intrinsic stresses in the pelvic floor. The governing differential equation for the deflection of the pelvic floor is written as:

$$\nabla^4\delta = \frac{P}{\alpha} + \frac{t}{\alpha\, r}\frac{\partial\phi}{\partial r}\frac{\partial^2\delta}{\partial r^2} \quad \text{and} \quad \nabla^4\phi = -\frac{E}{r}\frac{\partial\delta}{\partial r}\frac{\partial^2\delta}{\partial r^2} \quad (2)$$

where, ϕis the Airy stress function and ∇^4 is the biharmonic operator. Airy stress function reduces the generalized formulation to the governing equations with solvable unknowns. Similar to the FE model, the boundaries of the pelvic floor are assumed to be fixed with no displacements, which yields:

$$\delta|_{r=edge} = 0 \text{ and } \frac{\partial\delta}{\partial r}|_{r=edge} = 0 \quad (3)$$

An additional boundary condition of stretch λat the edge of the pelvic floor is assumed to be zero. The stretch is written in terms of the circumferential strain,(ε_θ) and residual strain (ε_r) is:

$$\lambda|_{r=a} = r\,(\varepsilon_\theta - \varepsilon_r)|_{r=a} = 0 \tag{4}$$

which yields the following differential equation:

$$\frac{\partial^2 \phi}{\partial r^2} - \frac{\nu}{r}\frac{\partial \phi}{\partial r} = \varepsilon_r E \tag{5}$$

The deflection and the Airy function have the following solutions:

$$\delta(r) = \delta_{max}(1 + C_1 r^2 + C_2 r^4) \text{ and } \phi = \delta^2_{max}\,(B_1 r^2 + B_2 r^4 + B_3 r^6 + B_4 r^8) \tag{6}$$

where δ_{max} is the maximum deflection of the pelvic floor. Applying the boundary condition (3) to eq (6), yields

$$\delta(r) = \delta_{max}\left[1 - \left(\frac{r}{a}\right)^2\right]^2 \tag{7}$$

which has similar dependence to the small deflection theory. Substituting (7) in the PDE (1) simplifies the generic Airy function in eq (6)

$$\phi(r) = \delta^2_{max}\left[B_1 r^2 - \frac{1}{4}\left(\frac{r}{a}\right)^2 + \frac{1}{9}\left(\frac{r}{a}\right)^6 - \frac{1}{48}\left(\frac{r}{a}\right)^8\right] \tag{8}$$

and invoking the stretch boundary condition (4) yields the airy function:

$$\phi(r) = \frac{\delta^2_{max} E}{12}\left[\left(\left(\frac{5-3\nu}{1-\nu}\right) + \left(\frac{\varepsilon_r}{2(1-\nu)}\right)\right)\left(\frac{r}{a}\right)^2 - \frac{1}{4}\left(\frac{r}{a}\right)^2 + \frac{1}{9}\left(\frac{r}{a}\right)^6 - \frac{1}{48}\left(\frac{r}{a}\right)^8\right] \tag{9}$$

The maximum deflection δ_{max} is solved by applying the Bubnov Galerking method by minimizing the governing differential equation (1) and assuming $\delta(r)$ is normal with respect to the coordinate functions.

$$\int_A \delta\left[\alpha\nabla^4\delta - \frac{t}{r}\left(\frac{\partial}{\partial r}\right)\left(\frac{\partial \phi}{\partial r}\frac{\partial \delta}{\partial r}\right) - P\right]dA = 0 \tag{10}$$

Integrating equation 10 gives

$$\frac{2Et(1+\nu)(23-9\nu)}{63a^2(1-\nu^2)}\,\delta^3_{max} + \frac{16\,E\,t^3}{9a^2(1-\nu^2)}\delta_{max} - \frac{Pa^2}{3} = 0 \tag{11}$$

The solution to δ_{max} is a cubic equation with three roots. The real roots of δ_{max} is:

$$\delta_{max} = \sqrt[3]{-\frac{\beta}{2} + \gamma} + \sqrt[3]{-\frac{\beta}{2} - \gamma}, \tag{12}$$

where

$$\gamma = \sqrt{\frac{\theta^3}{27} + \frac{\beta^2}{4}}, \qquad \theta = 14\,\frac{4t^2 + 3a^2\varepsilon_r(1+\nu)}{(1+\nu)(23-9\nu)},$$

$$\beta = \frac{-7\,Pa^4h^2}{8\alpha(1+\nu)(23-9\nu)}$$

The deflection at any point in the pelvic floor can be computed using eq (7). In this study, we use the maximum deflection for comparison with the FE results.

The analytical solution (eq. 12) is used to compute the evolution of maximum deflection with changes in the geometry of the pelvic floor. Three different geometric variations are considered: (a) changing the radius while keeping the mean thickness (6 mm) and pressure (4 kPa) constant, (b) changing the radius and thickness proportionately and (c) varying the radius, thickness and pressure proportionately. The analytical solution assumes an elastic material whose stiffness corresponds to the initial slope of the stress-stretch relation presented in Fig. S1 and a Poisson's ratio of 0.43 is used to represent a weakly compressible muscle tissue. A normalized dimension of 1 corresponds to the mean base model with a thickness of 6 mm. The horizontal axis represents the deviation from this normalized mean geometry, a value of 1.2 represents the radius, thickness and pressure scaled by a factor of 1.2. It can be observed from Fig. S1 that the deflection increases as a cubic function of the radius when all else being equal. However, when the thickness of the idealized pelvic floor is increased proportionately to the increase in the radius, the deflection increase showed a more linear increase for both the constant pressure and pressure scaled proportionately with the dimension. When the pressure is increased proportionately with the radius and thickness, the deflection increased at a rate of 2.5 times the increase in deflection when the pressure was kept constant. The pelvic floor displacement increases with increase in the size of the pelvic floor, even with a proportional increase in thickness. The increase in thickness is critical to minimize deflection especially at larger dimensions where a significant increase in the deflections are observed.

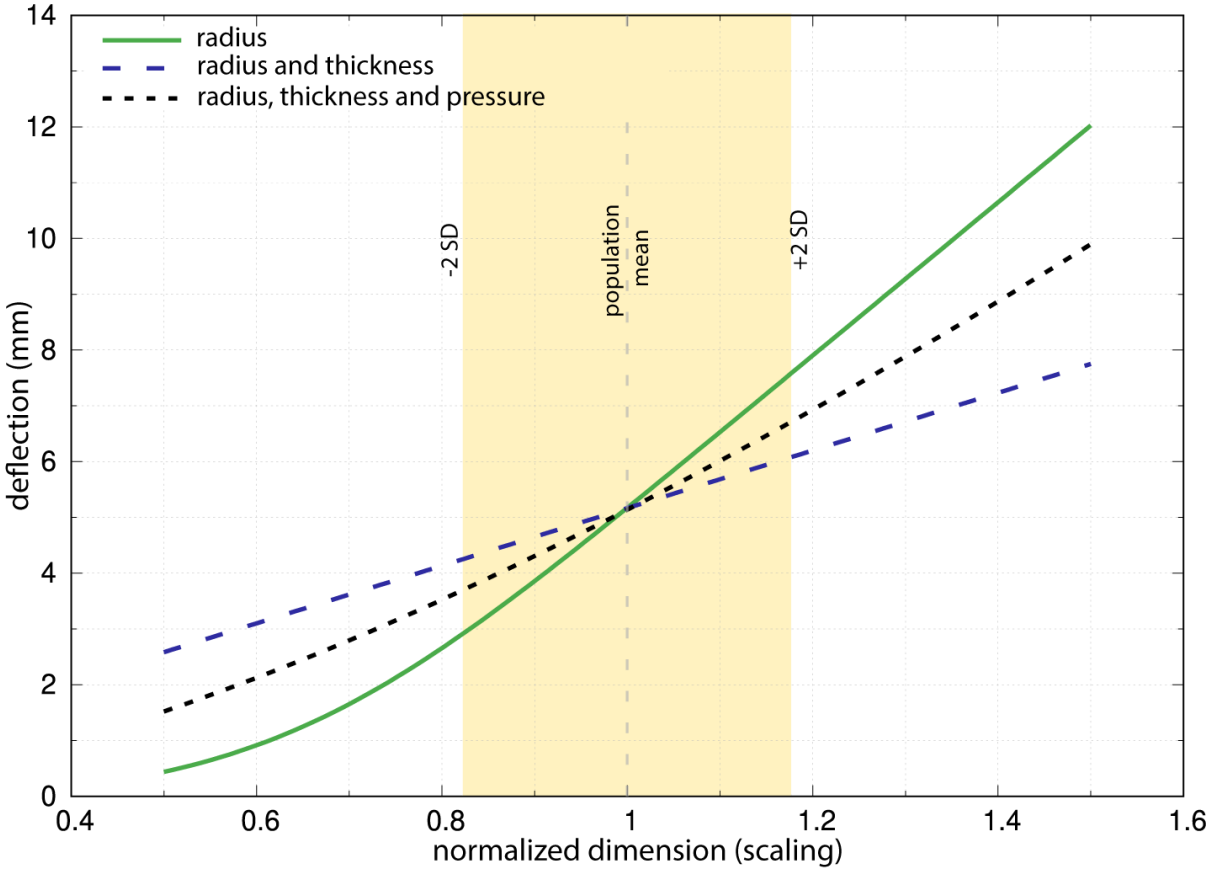

Fig. S1. An analytical solution using the Airy's stress function for the deflection of an idealized circular linear-elastic pelvic floor with a uniform thickness subjected to pressure. The three curves refer to the different combinations of parameters that were varied.

Results

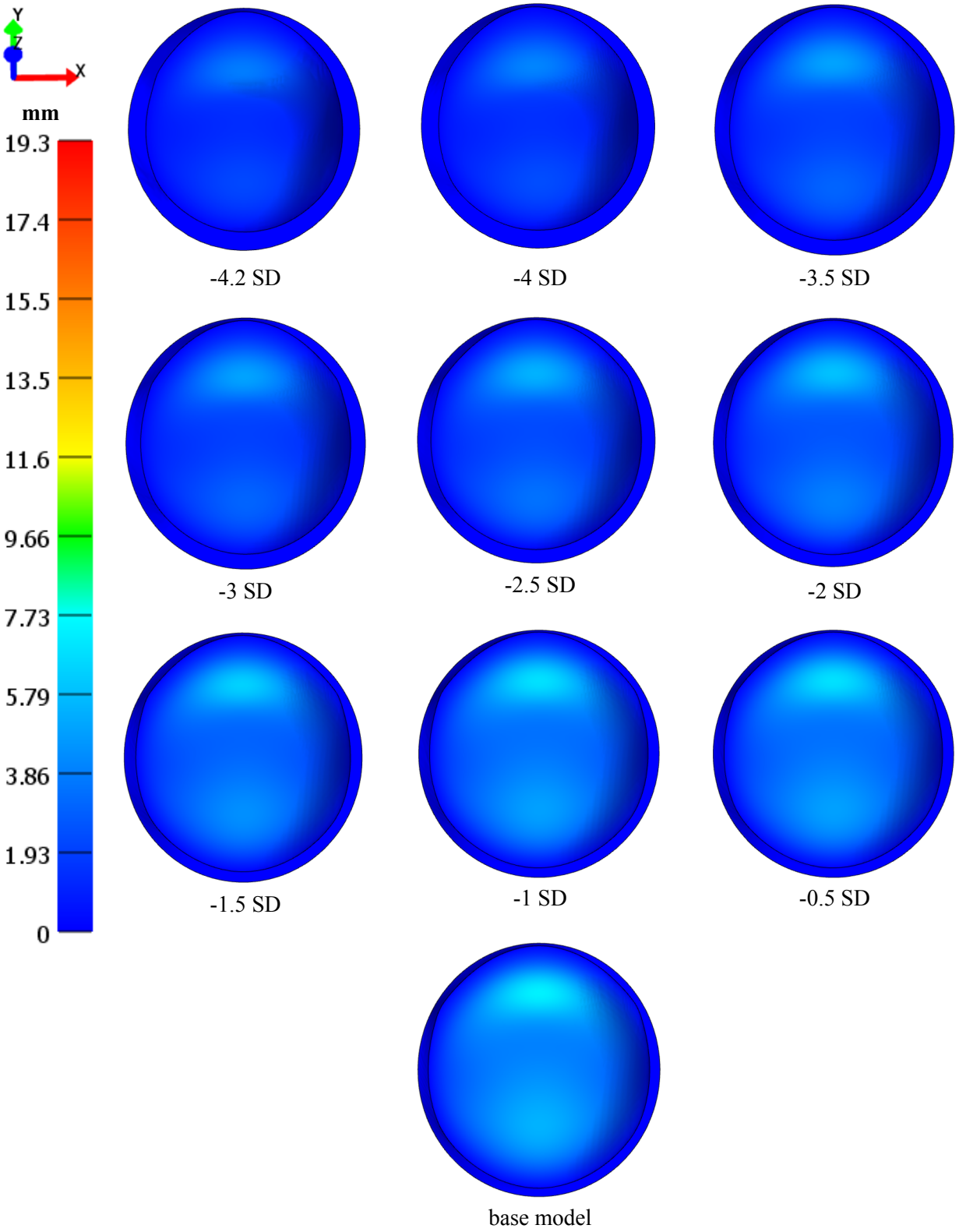
Y
Z
X
mm
19.3
17.4
15.5
13.5
11.6
9.66
7.73
5.79
3.86
1.93
0
-4.2 SD
-4 SD
-3.5 SD
-3 SD
-2.5 SD
-2 SD
-1.5 SD
-1 SD
-0.5 SD
base model

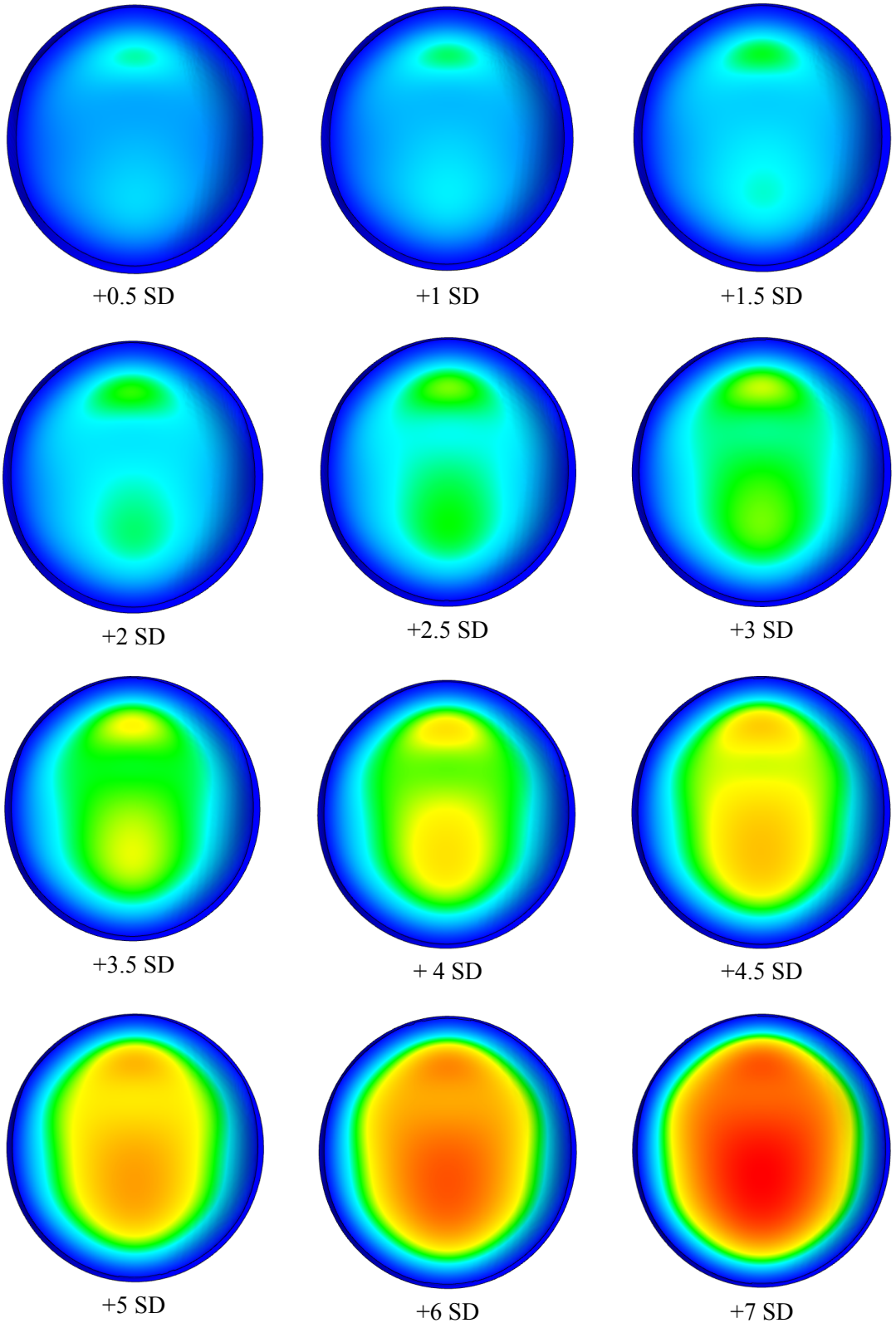

Fig. S2. Development of the displacement (in mm) in the anterior and posterior compartments when varying the average radius (constant thickness; experiment 1). Models are viewed from above (cranial view), and the posterior compartment of the pelvic floor is located towards the top of each figure.

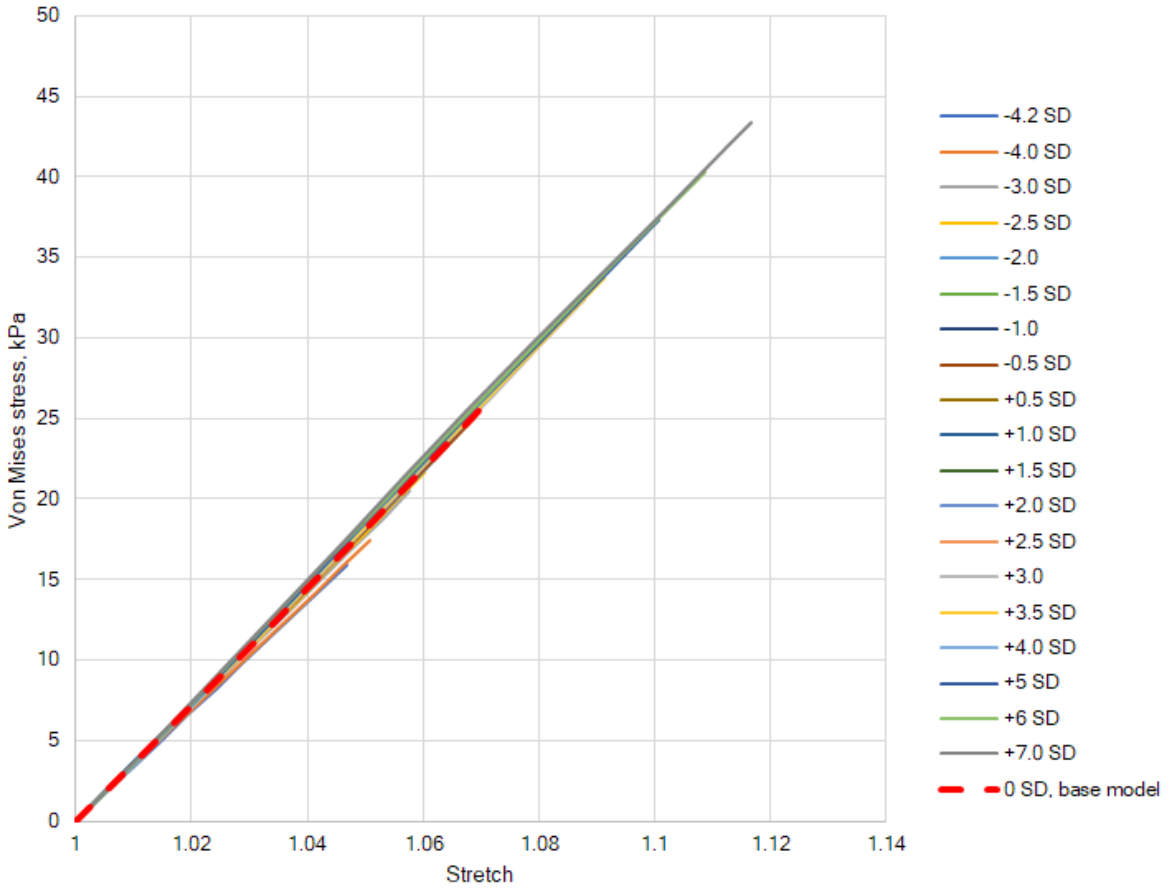

Fig. S3. The stress-stretch relationship for an increase in radius and constant thickness and pressure (4 kPa) in the anterior compartment (experiment 1).

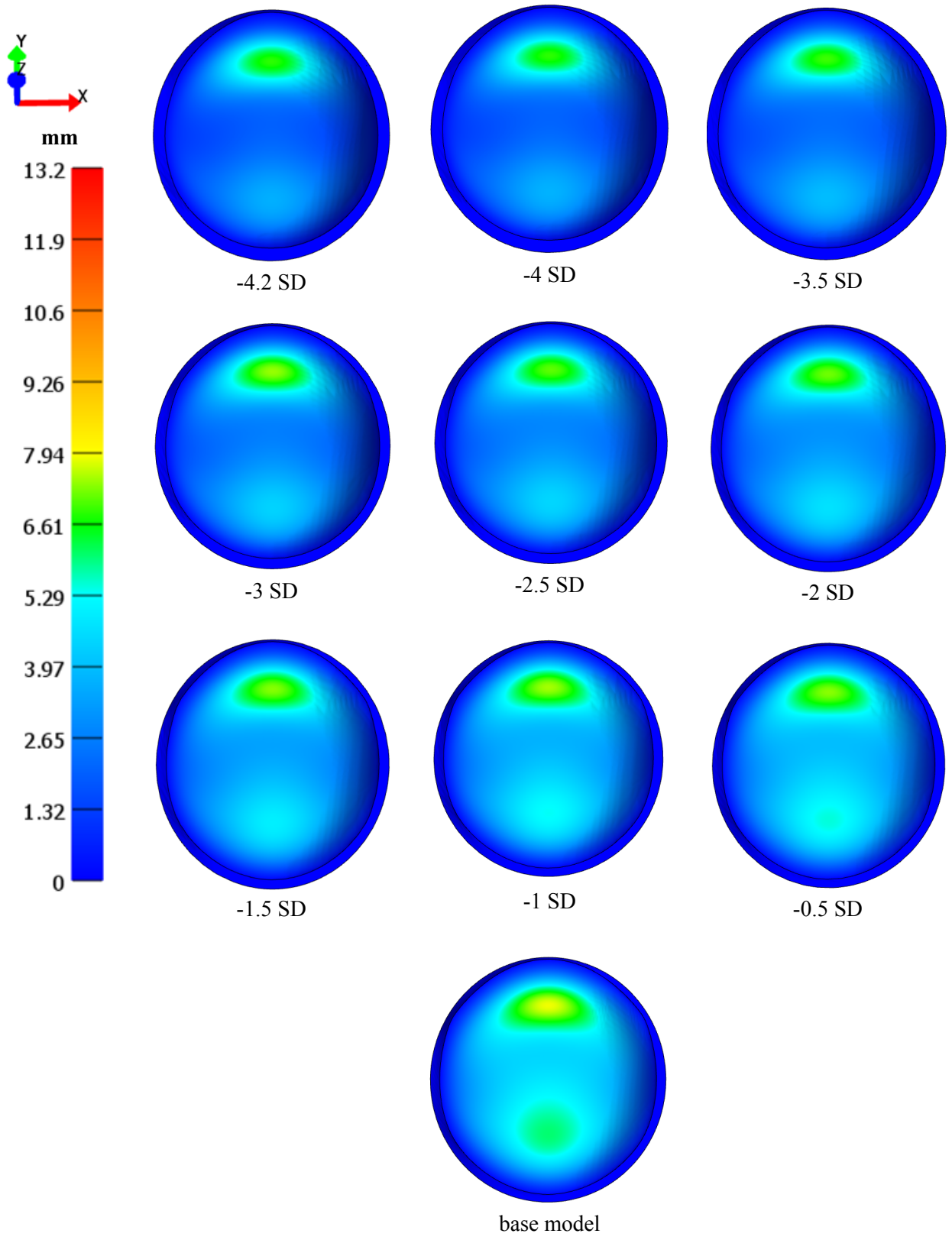
Y
Z
X
mm
13.2
11.9
10.6
9.26
7.94
6.61
5.29
3.97
2.65
1.32
0
-4.2 SD
-4 SD
-3.5 SD
-3 SD
-2.5 SD
-2 SD
-1.5 SD
-1 SD
-0.5 SD
base model

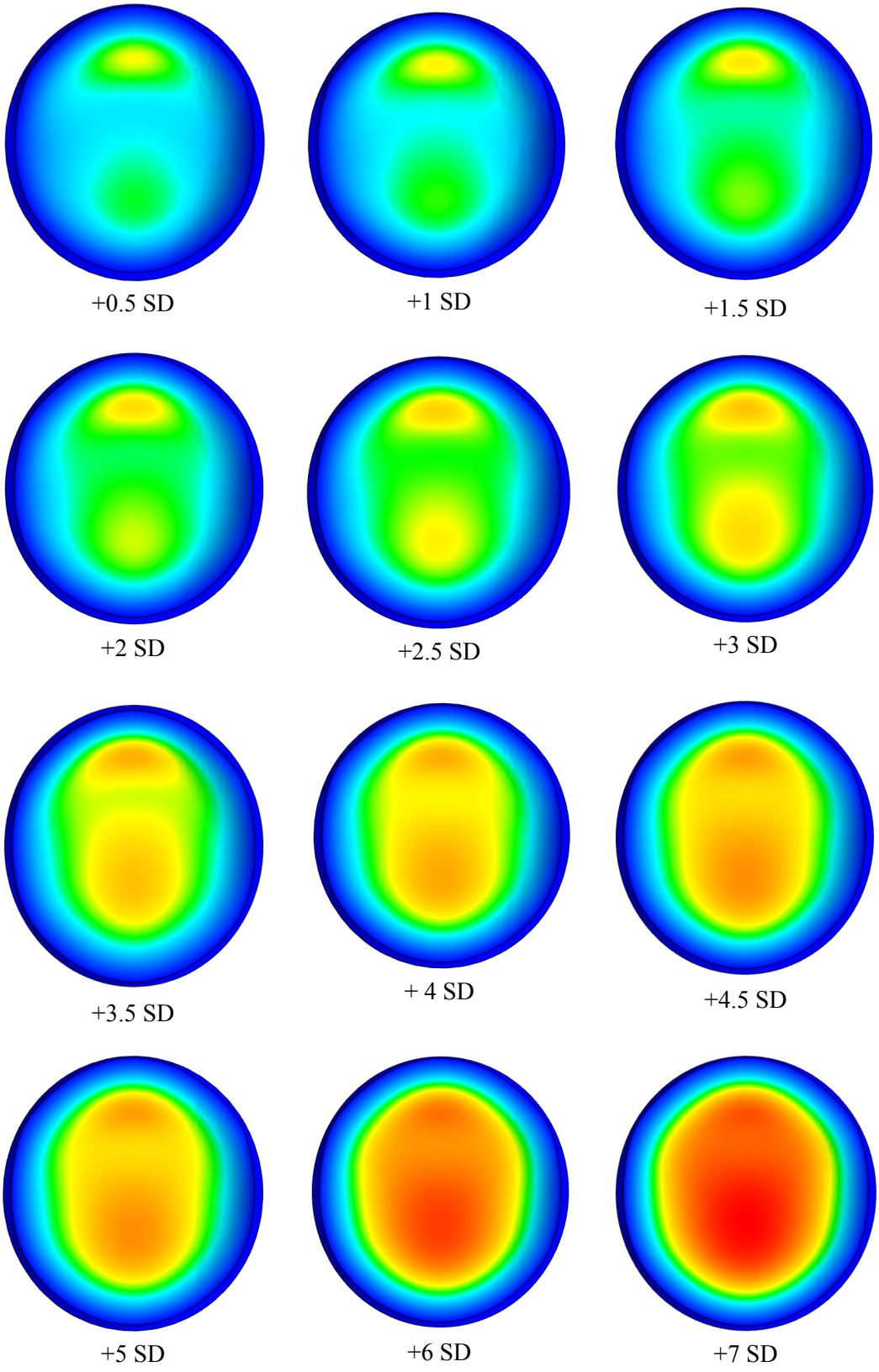

Fig. S4. Development of the displacement in the anterior and posterior compartments (in mm) when the radius and thickness are scaled proportionately (experiment 3). Models are viewed from above (cranial view) and the posterior compartment of the pelvic floor is located at the top of each figure.

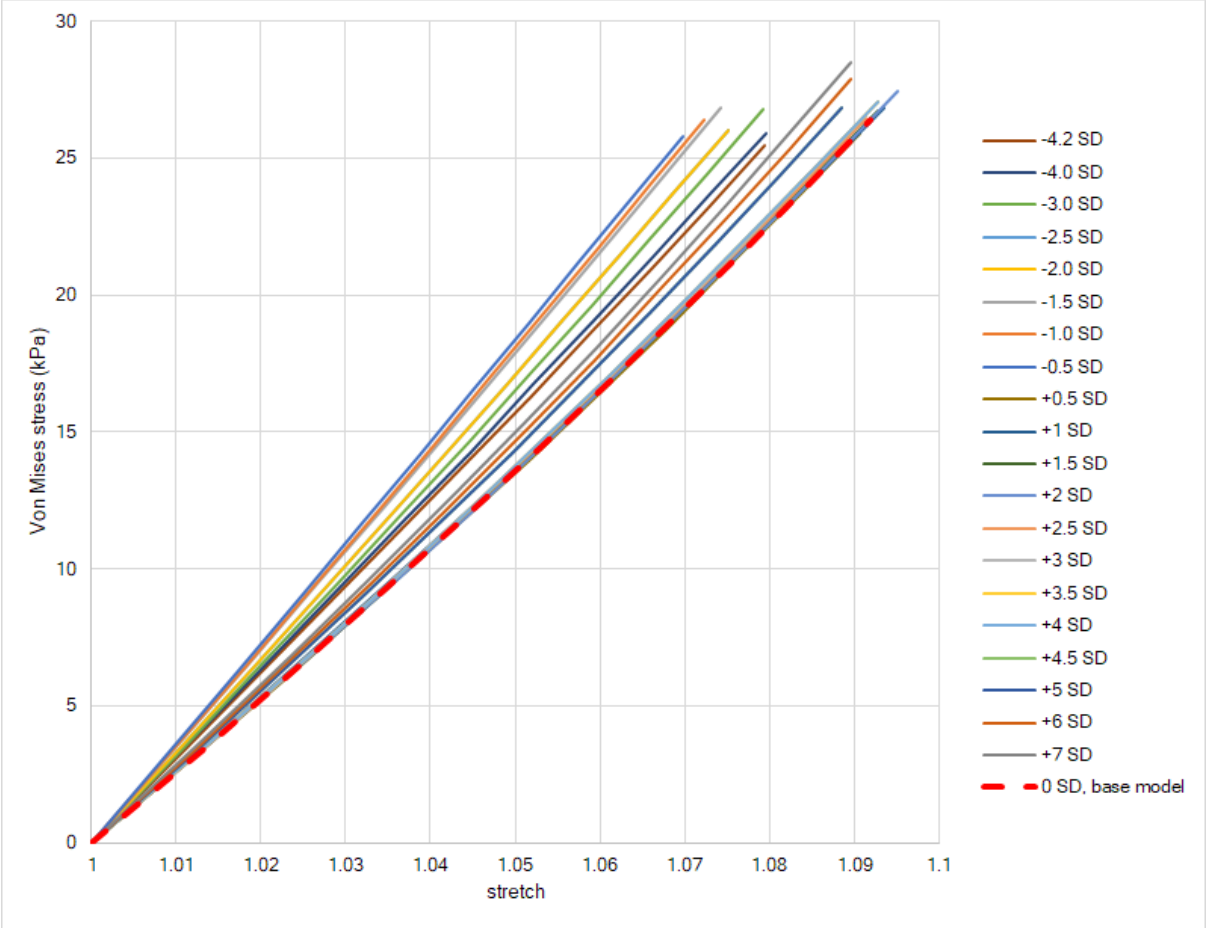

Fig. S5. The stress-stretch relationship for an increase in radius and proportionately scaled thickness at constant pressure (4 kPa) in the anterior compartment (experiment 3).

Further anatomical detail for levator ani group of muscles

The levator ani originates at the pubic bone and *arcus tendineus* and consists of several muscles (Fig. S6), for which we follow the nomenclature by Hershorn (2004). Relevant pelvic floor anatomy is briefly reviewed below.

The innermost fibres of the levator ani insert into the urethral sphincter, vagina and rectum, creating a continuous sheath of tissue (Fig. S6). Sphincter muscles are normally contracted for continence, whereas the vagina closure is maintained by the action of the intra-abdominal pressure and the levator ani muscle. The vertically oriented fibres that circle the back of the rectum belong to the puborectalis part of the levator muscle. It creates a sling around the rectum and plays an important part in faecal continence. Laterally to the puborectalis lies the pubococcygeus muscle, whose fibres pass almost horizontally and insert into the rectum and the coccygeal raphe. Finally, the lateralmost and the posterior part of the levator ani is composed of a thin layer of iliococcygeus and slightly thicker coccygeus muscles. The former originates on the *arcus tendineus*, while the latter originate on the ischial spines (left and right). Both are supported by fatty cushions underneath and insert into the last two vertebrae of the coccyx.

Different pelvic floor muscles vary in thickness (Fig. S6). Even within the levator ani, the puborectalis and pubococcygeus are considerably thicker than the iliococcygeus and coccygeus muscles. The medical literature reports thicknesses of the puborectalis muscle ranging from 6.23 mm to 8.12 mm (Table S1). The *in vivo* thickness of the posterior portions of the levator ani (e.g., the iliococcygeus) has not been studied in the same level of detail but has been reported to lie between 2.5

and 4 mm ^{2}. This, therefore, excludes muscles such as the *M. obturator internus* (Fig. S6), which are much thicker, but which are also less involved in continence and childbirth.

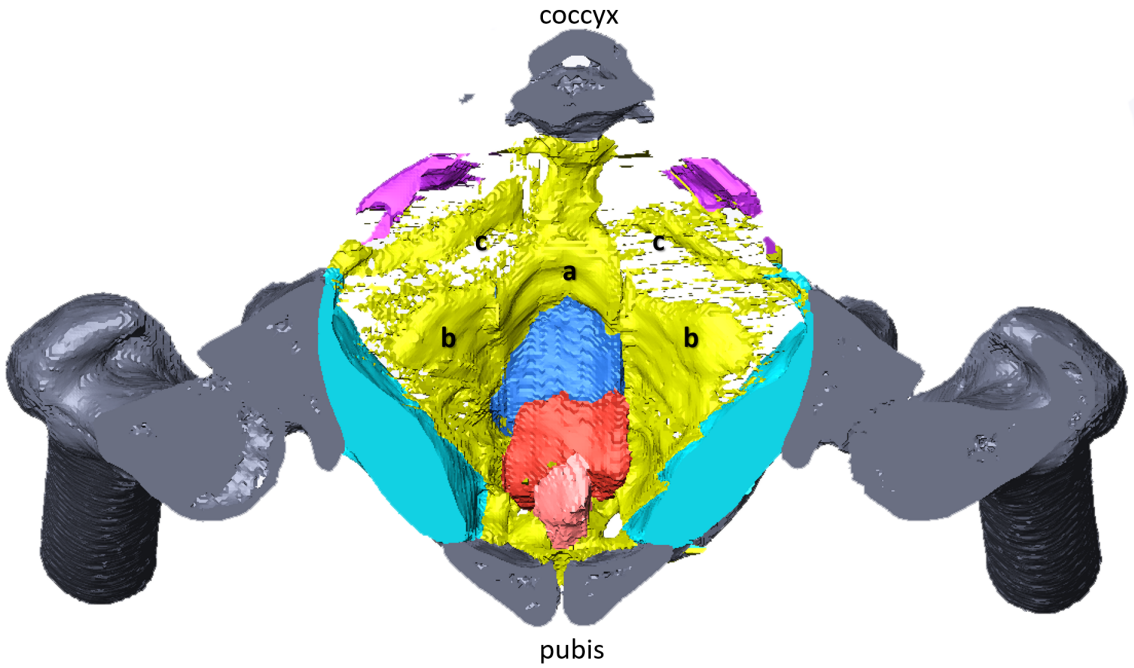

Fig. S6. The different pelvic floor muscles are shown in a transverse plane (coronal view), obtained by segmentation of a CT scan from the New Mexico Decedent Image Database. Skeletal elements are shown in grey, obturator internus in turquoise, piriformis (partial) in magenta, levator ani and urogenital membrane in yellow. Centrally, from the pubic bones towards the coccyx, the tissues of the urethra (pink), vagina (red) and rectum (blue) are visible. Three parts of the levator ani are marked: (a) puborectalis, (b) iliococcygeus, (c) coccygeus muscles. Note that the latter are very thin.

Table S1: Reported thickness of the pelvic floor muscles (non-exhaustive list of sources).

Publication	Method	Number of cases	Thickness in healthy women
Mørkved et al. 2004[3]	Perineal ultrasound	103	Urogenital diaphragm at relaxation 7.15±0.33 mm
Silva et al. 2017[4]	static MRI, transverse plane	4	Mid-vagina left 8.12±2.00 mm, right 7.29 ±2.28 mm; Anal canal left 5.20±1.27, right 5.68±1.78.
Yaşar et al. 2019[5]	static MRI, transverse plane	45	Puborectalis left 6.23±0.73, right 7.00±0.71
Hoyte et al. 2004[6]	static MRI	10	right anterior levator (min-max) 4.66 -10.01 mm; left anterior levator (min-max) 4.66-11.35 mm; right posterior levator (min-max) 2.00-8.00 mm; left posterior levator (min-max) 2.00-7.33 mm.
Dierick et al. 2018[2]	static MRI	17	mid-vagina iliococcygeus 3.7±0.38 mm mid-rectum iliococcygeus 3.95 ±0.4 mm mid-vagina puborectalis 9.15 ±0.68 mm mid-rectum puborectalis 8.35 ±0.9 mm

Finite element model and its validation

We adopted an isotropic Mooney-Rivlin model (eq. 13) to represent pelvic floor tissues with the following parameters: c_1=26 kPa, c_2=14 kPa [4] and the bulk modulus, K = 1000 kPa to reflect the near-incompressibility of the material[7].

$$W = c_1\left(I_1 - 3\right) + c_2\left(I_2 - 3\right) + \frac{1}{2}K(\ln J)^2 \quad (13)$$

Here, c_1 and c_2 are the Mooney-Rivlin material coefficients, I_1 and I_2 are the invariants of the deviatoric part of the right Cauchy-Green deformation tensor, and J is the Jacobian of the deformation.

The Cauchy stress for the Mooney-Rivlin material under uniaxial loading depends on the stretch (λ) as

$$\sigma_{Mooney} = 2\left(\lambda^2 - \frac{1}{\lambda}\right)\left(c_1 + c_2\frac{1}{\lambda}\right) \quad (14)$$

where stretch (λ) is defined as the ratio of the deformed length over the original length.

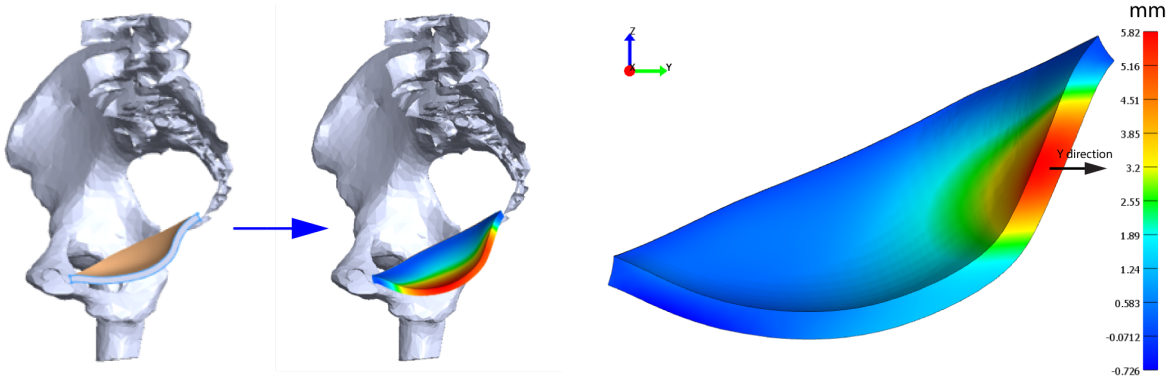

a. **b.**

	Displacement (mm)	
	dMRI (Silva et al. 2017)[4]	**FE base model**
Y (horizontal)	6.235±4.004	5.729
Z (vertical)	4.495±1.560	5.409

c.

Fig. S7. FE model validation. (a) The overall change in shape upon application of the pressure to the superior surface of the model. (b) Plot of the displacement of the posterior compartment in the horizontal (Y) axis (in mm). We exported the maximum displacement of several elements at the outer surface of the posterior compartment in the region of maximum displacement, from which we computed an average. (c) dynamic MRI (dMRI) and modeled Y and Z average displacements of the posterior compartment for the base model.

Experiments

Table S2: Experiments and models. Measurements are given in mm. Abbreviations: ML – mediolateral, AP – anteroposterior, SD – standard deviation from the mean.

		ML	AP	thickness	
	Average	53	56	6	**Base Model**
	SD	4.5	4.8	NA	

Experiment 1. Changing average radius				**Experiment 2. Changing thickness**			**Experiment 3. Changing radius and thickness proportionately**			
SD factor	ML	AP	thickness	ML	AP	thickness	SD factor	ML	AP	thickness
-4.2	34.1	35.84	6	53	56	1	-4.2	34.1	35.84	3.89
-4	35	36.8	6	53	56	2	-4	35	36.8	4.07
-3.5	37.25	39.2	6	53	56	3	-3.5	37.25	39.2	4.31
-3	39.5	41.6	6	53	56	4	-3	39.5	41.6	4.55
-2.5	41.75	44	6	53	56	5	-2.5	41.75	44	4.79
-2	44	46.4	6	53	56	6	-2	44	46.4	5.03
-1.5	46.25	48.8	6	53	56	7	-1.5	46.25	48.8	5.28
-1	48.5	51.2	6	53	56	8	-1	48.5	51.2	5.52
-0.5	50.75	53.6	6	53	56	9	-0.5	50.75	53.6	5.76
0	53	56	6	53	56	10	0	53	56	6.00
0.5	55.25	58.4	6	53	56	11	0.5	55.25	58.4	6.24
1	57.5	60.8	6	53	56	12	1	57.5	60.8	6.48
1.5	59.75	63.2	6				1.5	59.75	63.2	6.71
2	62	65.6	6				2	62	65.6	6.97
2.5	64.25	68	6				2.5	64.25	68	7.21
3	66.5	70.4	6				3	66.5	70.4	7.45
3.5	68.75	72.8	6				3.5	68.75	72.8	7.69
4	71	75.2	6				4	71	75.2	7.94
4.5	73.25	77.6	6				4.5	73.25	77.6	8.18
5	75.5	80	6				5	75.5	80	8.42
6	80	84.8	6				6	80	84.8	8.91
7	84.5	89.6	6				7	84.5	89.6	9.40

References

1. Timoshenko, S. P. & Woinowsky-Krieger, S. *Theory of plates and shells*. (McGraw-hill, 1959).
2. Dierick, F. *et al.* Clinical and MRI changes of puborectalis and iliococcygeus after a short period of intensive pelvic floor muscles training with or without instrumentation: A prospective randomized controlled trial. *Eur. J. Appl. Physiol.* **118**, 1661–1671 (2018).
3. Mørkved, S., Salvesen, K. A., Bø, K. & Eik-Nes, S. Pelvic floor muscle strength and thickness in continent and incontinent nulliparous pregnant women. *Int. Urogynecol. J. Pelvic Floor Dysfunct.* **15**, 384–9; discussion 390 (2004).

4. Silva, M. E. T., Brandão, S., Parente, M. P. L., Mascarenhas, T. & Natal Jorge, R. M. Biomechanical properties of the pelvic floor muscles of continent and incontinent women using an inverse finite element analysis. *Comput. Methods Biomech. Biomed. Engin.* **20**, 842–852 (2017).
5. Yaşar, L., Telci, S. O., Doğan, K., Kaya, E. & Ekin, M. Predictive role of measurement of pelvic floor muscle thickness with static MRI in stress and mixed urinary incontinence. *Int. Urogynecol. J.* **30**, 271–277 (2019).
6. Hoyte, L. *et al.* Levator ani thickness variations in symptomatic and asymptomatic women using magnetic resonance-based 3-dimensional color mapping. *Am. J. Obstet. Gynecol.* **191**, 856–861 (2004).
7. Maas, S. A., Ellis, B. J., Ateshian, G. A. & Weiss, J. A. FEBio: finite elements for biomechanics. *J. Biomech. Eng.* **134**, 011005 (2012).